

3D Numerical Investigation of Bio-Inspired Vertical Axis Wind Turbine Rotor using Arbitrary Mesh Interface (AMI)

Manu Aryal¹, Manabendra M. De², and Chandan Bose³

¹Graduate Research Scholar, Dept. of Mechanical and Aerospace Engineering, IOE Pulchowk Campus, Tribhuvan University, NEPAL

²Assistant Professor, Academy of Scientific and Innovative Research (AcSIR), New Delhi, INDIA and Senior Principal Scientist, CSIR-National Aerospace Laboratories (NAL), Bengaluru, Karnataka, INDIA

³Assistant Professor, Aerospace Engineering, College of Engineering and Physical Sciences, The University of Birmingham

July 14, 2025

Synopsis

This study presents a 3D numerical investigation of bio-inspired vertical axis wind turbine rotors using the Arbitrary Mesh Interface (AMI) methodology in OpenFOAM v-2412. The AMI approach addresses limitations of Multiple Reference Frame (MRF) method for geometries where cross sectional change affects the fluid interaction particularly in single blade savonius rotors where frontal shape changes with azimuth orientation. This improvement of AMI over MRF approach comes at an expense of computational time.

The framework utilizes a sliding mesh technique with prescribed rotational motion to the rotating region in the domain. A conservative interpolation of mass and momentum across the non-conformal AMI cyclic interfaces utilizes area-weighted averaging while maintaining flux conservation and numerical stability. The solidBodyMotionSolver with rotatingMotion function drives the inner rotatingZone while the cyclicAMI boundary conditions handle periodic coupling between the interfaces.

This methodology successfully captured the dynamic torque variations and unsteady flow physics around a bio-inspired rotor shape based on a seedpod with height to diameter ratio of 3.66 under laminar flow conditions ($Re = 48000$). The study revealed that bio-inspired rotors could achieve better startup characteristics. Torque characterization revealed the major difference of single peak patterns with maximum torque at 0° orientation for bio-inspired rotors while savonius rotors have double peak patterns with peaks at 45° and 225° . Lower thrust coefficients indicated significantly reduced structural loading for bionic turbines.

The investigation revealed that bio-inspired rotors can be the optimal energy solutions for urban locations due to superior startup characteristics at low wind conditions, stable performance across varying Reynolds numbers, and reduced vibration from single-peak torque patterns. Conventional Savonius rotors excel in higher peak power coefficients but require stronger support structures due to elevated thrust loads.

Keywords: Vertical Axis Wind Turbine, Bio-inspired Design, Arbitrary Mesh Interface, OpenFOAM, Computational Fluid Dynamics, Savonius Rotor

1 Introduction

Extracting energy from nature without harmful consequences to the nature has always been of human interest and motivating the research advancements in the field of renewable energy. The potential of wind energy along with the simplicity of Savonius type rotors has inspired research on Vertical Axis Wind Turbines (VAWTs) and its modifications to maximize the power yield or optimize its performance further. These drag type rotors can operate fairly well in the low speed conditions without requiring intricate engineering design. But the conventional Savonius rotor blades are notorious for low operating efficiency and cases of reverse torque, hampering its intended purpose. Attempts to improve the design by introducing multi-blade rotors, increasing stages, tweaking the shapes, and adding components such as guide vanes and nozzles have been carried out through the times. [1]. The parameters like overlap ratios and blade edge conditions show sensitivity on the performance of these drag type rotors across various Reynolds numbers. [2]. Increase in overall surface area of the wind structure interaction increases the drag surfaces against the wind flow and results in reversed torque decreasing the net moment in the turbine rotor. So, two bladed Savonius rotors, having more effective area, providing maximum power [3].

Burcin et al. experimentally studied the effects of modifications on blade end design and improvements in the power coefficient. [4] At low speeds and models where negative torque causes reduced turbine efficiency, placing guide vanes around the rotor negates these detrimental effects. [5] Kamoji et. al through the study of modified Savonius rotor figured out the value of coefficient of power 0.21 with a Savonius rotor with no overlap, arc angle of 124° and an aspect ratio of 0.7 which is 10.5% improvement upon traditional rotor of same configuration. [6]

A shift from conventional Savonius rotor designs showed helical rotors, twisted-bladed rotors and shape modifications. Numerical investigations on a Helical rotor with 180° twist resulted in these blades being highly sensitive to the Reynold's numbers of the wind. Still the performance of the helical blade was higher than the conventional Savonius rotor. [7] 2D numerical investigations on various blade profiles such as semicircular, Benesh, modified Bach and elliptical profiles along with experimental verifications indicated ellipticals being the ones with highest C_p . [8] WA Elsakry's work on 450 twisted rotors combined with varying overlap ratios, aspect ratios and wind velocities shows a 75.3% increase in performance over conventional Savonius rotors. [9] [10]. Integration of biologically inspired designs for the rotors has unlocked a new domain for research and potential for the VAWT rotor performance. Progressive work towards these bio-inspired models for both Darrius type and Savonius type rotors have been done in this past decade. Priya et al. recreated the helical structures of Mimosa and Bauhinia Variegata seed pods as a single bladed Savonius rotor taking the d/h and p/h ratios as reference. These rotors showed encouraging startup tendencies at low speed conditions of 2 m/s. [11] Aerodynamic behaviour along with the structural stresses developed in

the maple seed inspired Darrieus type rotor blades showed minimum wake effects along with low stresses. [12] [13].

In case of drag type rotors, a fibonacci spiral inspired blade contour improved the conventional Savonius turbine performance by 14-30%. [14]. However, these works fail to explain the performance of nature-based Savonius rotor designs and the low torque requirements for operation. Also, there are sparse studies carried out on the aerodynamic performance of bio-inspired drag type VAWT rotors. For small-scale urban power generation, these easy startup turbine blade geometries are the way forward and thus requiring further research in this area.

This study carries out the 3D investigation of the seed pod inspired vertical axis wind turbine rotor building up on the work by Priya et al. to further elaborate the startup abilities of this kind of single blade helical geometry. The replica of a bionic model is compared with a modified model to observe the effects of modification on the performance. Variation of the power coefficients, thrust coefficients, and torque coefficients with the tip speed ratio can provide fresh insights on the operation and power generation from these types of small-scale power plants. The optimal TSR of operation will be substantial to define the urban applications with low wind conditions for this kind of turbine design. A dynamic meshing approach with rotating arbitrary mesh interface (AMI) coupled with the traditional finite volume computations has provided the foundation for the numerical investigation side of this study. OpenFOAM v-2412 was used to carry out the simulations while the blockMesh and snappyHexMesh utilities were used for mesh generation purposes.

This paper is structured as follows, the computational methodology describes in detail the physics solved by the numerical framework along with the techniques used for meshing and the dynamic simulation. The solver specifications followed by a proper validation with existing experimental literature is covered in this section. The results of the numerical investigation along with the supporting graphics and their interpretations is reported in the results and discussion section. Conclusion summarizes the answers to the research questions based on the outcomes of this study.

2 Computational Methodology

For 3D investigation of the rotor performance, a computational domain 11 times the maximum diameter of the rotor was taken. This number was taken after the domain size independence study. A rotating region is defined within the flow domain as a cylinder of diameter 2 times that of rotor and the height equal to the domain height, equivalent to the geometry of rotor.

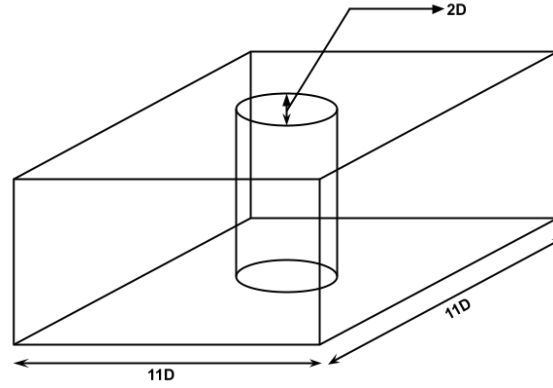


Figure 1: Computational Domain

2.1 Dynamic Modeling Approach

To model rotating bodies, various methods can be used based on the type of motion to be modelled. For rigid body motion, a dynamic sliding mesh with a 6 DoF rigid body motion solver is used. The model responds to the loads acting on the body due to the fluid and gravity forces. In order to model prescribed motion of a rotating body in OpenFOAM, multiple approaches such as Multiple Reference Frame (MRF) method, Arbitrary Mesh Interface (AMI) method, Overset Mesh etc can be used.

For this case, initially the MRF method was opted for its simplicity and computational viability. In the Multiple Reference Frame method of dynamic solving, the reference frame of the rotating region is defined in a way such that the fluid equations solve for relative velocity rather than absolute local velocity. This relative velocity is a vector addition of the local linear velocity and rotational velocity such that there is no need to deform the mesh in order to account for rotation. However this is a pseudo transient approach where the change in fluid interaction behaviour due to the geometry rotation is not considered. For the cases where the orientation of the cross section of interaction does not change with progressing time such as in Horizontal Axis Wind Turbines (HAWTs), or other rotating bodies with high number of blades like propellers or ship hulls, the MRF approach is viable for rudimentary estimation of the properties. A periodic cyclic boundary in complement to the MRF can provide highly accurate results.

To model the flow behavior and forces in geometries where the dynamic nature of the motion changes the geometry interface and that needs to be accounted for to estimate performance, MRF approach is not sufficient, e.g. in Savonius type VAWT rotor the frontal shape of rotor is dynamic so solving for one orientation is not enough to accurately estimate the response of other orientations. Hence, AMI method of dynamic motion solving is opted for in this study. This is a sliding mesh approach where the fluid domain is split into a rotating region with rotating geometry and the outer domain is stationary. The inner region rotates with a prescribed angular rotation and the transfer of field variables across AMI interfaces between the interacting regions using several interpolation schemes. The interpolation weightage is done such that each pair of source and target faces have included the neighbouring faces with connected edges. This accounts for almost half the cost of AMI. Various methods are implemented to streamline this procedure [15]. AMI avoids mesh deforming near the turbine rotor blades, reducing the errors due to deformed cells.

2.2 Arbitrary Mesh Interface (AMI) approach

Arbitrary Mesh Interface (AMI) utility of dynamic meshing was used to create the sliding mesh interface where the inner cylindrical region rotates with a prescribed angular velocity based on the tip speed ratio.



Figure 2: Rotation of the AMI region in a prescribed direction

This is a transient simulation as the blade rotates with respect to the incoming flow, so an incompressible transient solver, `pimpleFoam` is used as it is best suited for this flow behavior. `pimpleFoam` combines the PISO and SIMPLE algorithms to generate time-accurate pseudotransient steady-state simulations making it essential for solving complex flow problems. The solver primarily solves the continuity equation (1) and momentum equation (2) otherwise known as the Navier-Stokes equation to model the flow physics. Since the overall flow will be at a low Reynolds number, turbulence modeling was not used assuming the flow to be laminar.

$$\nabla \cdot u = 0 \quad (1)$$

$$\frac{\partial u}{\partial t} + \nabla(uu) = -\nabla p + \nu \nabla^2 u \quad (2)$$

The AMI technique couples these non-conformal interfaces between the moving and stationary domains. The conservative variables (mass and momentum) are interpolated across the sliding interface for accurate information transfer.

$$\Phi = \sum_{i \in source} \phi_i A_i \cdot n_i \rightarrow \sum_{j \in target} \phi_j A_j \cdot n_j \quad (3)$$

The interpolation generally utilized area-weighted averages or least squares to conserve the flux across the surface, in order to ensure numerical stability.

The results from the solver will be used to analyze the performances of the wind turbine rotors by comparing the non dimensional attributes coefficient of power(C_p), coefficient of torque(C_q), and coefficient of thrust(C_T). Coefficient of power indicates the efficiency of power extraction from the wind with respect to the available kinetic energy in the flow.

$$C_p = \frac{Power}{\frac{1}{2}\rho AV^3} \quad (4)$$

Non dimensional torque or the coefficient of torque is the parameter used to predict and scale the performance.

$$C_q = \frac{Torque}{\frac{1}{2}\rho AV^2 R} \quad (5)$$

Coefficient of thrust is the indicator used to assess the lift/drag efficiency of rotor design by non dimensionalizing the thrust.

$$C_T = \frac{Thrust}{\frac{1}{2}\rho AV^2} \quad (6)$$

These parameters are compared against another dimensionless number, Tip Speed Ratio (TSR) which is the speed of tip of the wind turbine rotor with respect to the flowing wind.

$$TSR(\lambda) = \frac{\omega * R}{V} \quad (7)$$

2.3 Geometry and Setup

Mimosa and Bauhinia Variegata seed pod inspired seed pod geometries are extracted from the work by P. Venkataraman et al. along with the modifications as seen in the Figure 3. [11]

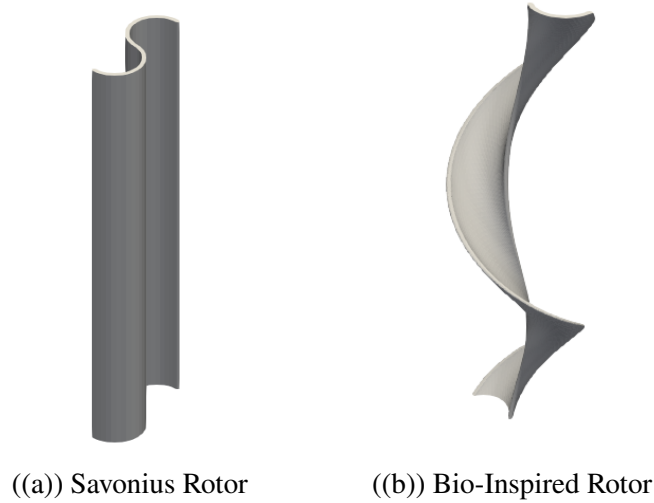


Figure 3: CAD Geometries

The H/D ratio of all these rotors is consistent with a height of 300 mm and a diameter of 82 mm. For the rotating region, the diameter of the cylinder is 164 mm and the domain size is 5D on each side apart from the height region. *blockMesh* creates hexahedral cells throughout the domain and then *snappyHexMesh* first of all castellates the mesh elements which are in contact with the geometry on various predefined levels and snaps these mesh edges on the geometry surface to generate the

flow domain consisting of rotating turbine region with refined mesh. The geometry then snaps along with the static outer region with structured but relatively coarse mesh as seen in Figure 4.

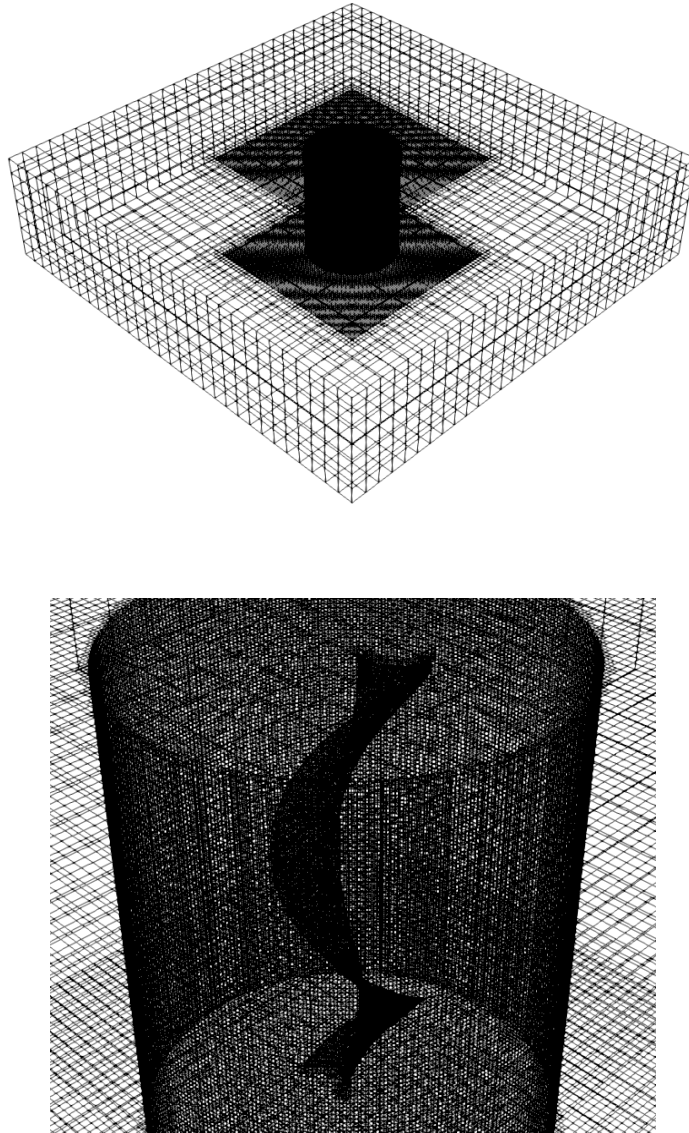


Figure 4: Computaional Domain Mesh

The flow domain consists of inlet, outlet, walls and frontAndBack patches. For the interface between static and rotating regions with non conforming mesh, *cyclicAMI* boundary which is best suitable for periodic rotating geometries is used. The flow is laminar which excludes the turbulence modeling. Only pressure and velocity boundary conditions are required to be defined and solved.

Table 1: Initial and Boundary Conditions

Patch	p	U
inlet	zeroGradient	fixedValue uniform (5 0 0)
outlet	fixedValue uniform 0	zeroGradient
lowerWall	zeroGradient	zeroGradient
upperWall	zeroGradient	zeroGradient
savonius	fixedFluxPressure uniform 0	movingWallVelocity uniform (0 0 0)
frontAndBack	zeroGradient	zeroGradient
AMI1	cyclicAMI uniform 0	cyclicAMI uniform (0 0 0)
AMI2	cyclicAMI uniform 0	cyclicAMI uniform (0 0 0)

2.4 Dynamic Mesh Settings

The inner cylinder containing the rotor rotates with a prescribed angular rotation about the axial direction and the AMI interpolation happens between the subsequent overlapping faces of the mesh. solidBody motion solver from the fvMotionSolvers library provides the rotationMotion function to the inner rotatingZone.

Table 2: AMI Setup

Parameter	Value
dynamicFvMesh	dynamicMotionSolverFvMesh
motionSolverLibs	fvMotionSolvers
motionSolver	solidBody
cellZone	rotatingZone
solidBodyMotionFunction	rotatingMotion

2.5 Discretization Schemes and Solvers

The continuous fluid flow domain is broken down into a discrete set of elements and points to enable numerical solutions of the fluid dynamics equations. Various terms of the momentum equation are discretized differently based on the schemes on Table 3.

Table 3: Discretization Schemes

Parameters	Definition	Algorithm
ddtSchemes	default	Euler
gradSchemes	default	Gauss linear
divSchemes	div(phi,U)	Gauss linearUpwind grad(U)
	div(phi,k)	Gauss linearUpwind grad(U)
	div(phi,omega)	Gauss linearUpwind grad(U)
	div((nuEff*dev2(T(grad(U)))))	Gauss linear
laplacianSchemes	default	Gauss linear corrected
interpolationSchemes	default	linear
snGradSchemes	default	corrected
wallDist	method	meshWave

Following the discretization, solvers and algorithms use numerical methods to iteratively solve the discretized fluid dynamics equations within the predefined tolerance or to the specific run time. For different variables, several solvers were employed.

Table 4: Solvers

Parameters	(p pcorr)	(p pcorr)Final	U	UFinal
solver	GAMG	GAMG	smoothSolver	smoothSolver
smoother	DICGaussSeidel	DICGaussSeidel	symGaussSeidel	symGaussSeidel
tolerance	1e-06	1e-06	1e-06	1e-06
relTol	0.1	0	0.1	0

The PIMPLE algorithm, a combination of Pressure Implicit with Splitting of Operator (PISO) and SIMPLE (Semi-Implicit Method for Pressure Linked Equation) is the iterative solver that is used for solving the transient cases which is well suited for this case.

```

PIMPLE
{
    momentumPredictor    yes;
    nOuterCorrectors      3;
    nCorrectors           1;
    nNonOrthogonalCorrectors 0;
}

```

Figure 5: PIMPLE Algorithm

2.6 Computational Parameters and Convergence

Adaptive step stepping adjacent to 0.5 courant number maintained the numerical stability of the simulation. For convergence in each time step, a residual limit of $< 1e-6$ was used for each variable.

The inlet flow was kept constant at 5 m/s and the rotation velocity was altered to change the TSR of the flow.

The temporal moment data obtained from the simulation had to be numerically integrated over the stable time steps using trapezoidal algorithm within Python numpy library to obtain the cycle averaged torque which was multiplied with angular velocity to obtain the power

$$Power = Torque \cdot \omega \quad (8)$$

Reynolds number sensitivity of the flow at the constant TSR also needs to be studied which was done by varying the parameter μ (Viscosity of the flow) as change in velocity needs to be accommodated by changing the ω to keep TSR constant. This study only needs to be done for TSR cycles where the power output is maximum.

$$Re = \frac{\rho v L}{\mu} \quad (9)$$

Adjacent to nominal flow Reynolds number of 48000, further analysis was carried out to see the effects within ± 40000 range of flow.

2.7 Solver Validation

Experimental results of a two blade savonius turbine rotor blade conducted by Mohammad Hadi Ali was recreated using the defined solver for the validation of the setup. [3]

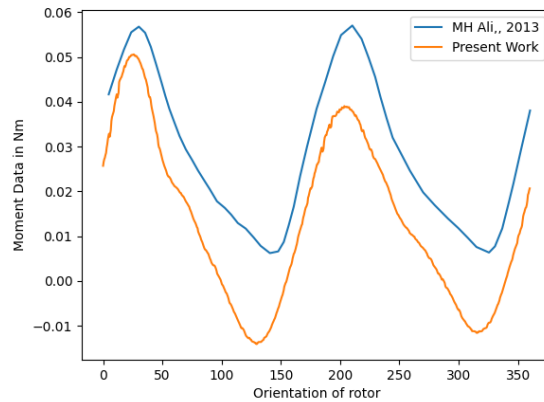


Figure 6: Validation of Solver

Figure 6 shows some difference in the amplitude of torque generated between the experimental and numerical data. Since the end caps were not modeled and the simulation model was limited to the height of turbine blade on the y-axis, this difference in result can be expected. However, the nature and range of thrust data are in coherence with the experiment.

3 Results and Discussions

The performance of drag-type wind turbines alters with the change in flow conditions. This variation has been studied by comparing the moment, power, and thrust performance of the rotor blade against the non dimensional tip speed ratio (λ). For different blade designs, the TSR where the power output is maximum is different. The numerical investigation of the rotors was carried out using the validated OpenFOAM solver on various TSRs by altering the rotational velocity of the prescribed motion while keeping the inflow speed constant.

When the tip speed ratio increases, the power output of the turbine increases, as presented in all the existing literature but after culmination, the C_p decreases with increase in TSR . So there exists an optimum wind velocity where the performance of a vertical axis wind turbine rotor is maximum. The results from the simulations indicate that the nature of C_p vs TSR curves is different for Bionic rotor as compared to the Savonius rotor as seen in Figure 7 and Figure 8.

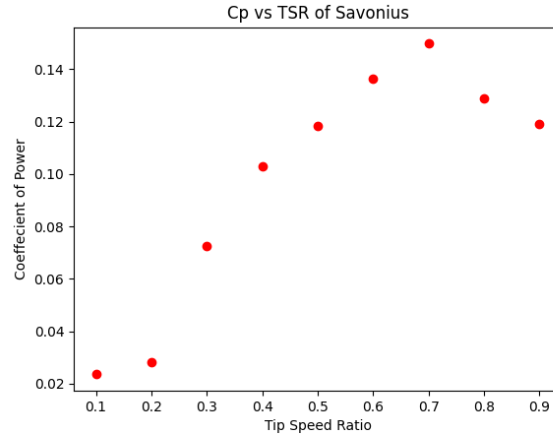


Figure 7: C_p vs TSR of Savonius Rotor

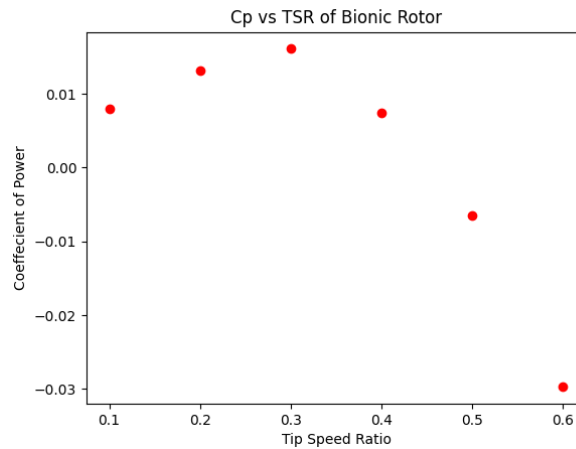


Figure 8: C_p vs TSR of Bionic Rotor

This clearly depicts the higher power output of savonius rotors at high speed applications but

for low speed conditions, Bionic rotors reach their apex power quickly indicating easy startup capabilities making it much suited for low speed urban applications.

Table 5: Performance of Savonius Rotor

TSR	Savonius		
	C_p	C_t	C_q
0.3	0.08763	1.6202	0.29211
0.4	0.12421	1.3202	0.31054
0.5	0.14273	1.3624	0.28547
0.6	0.1645	1.3522	0.27417
0.7	0.1806	1.36012	0.25799
0.8	0.15542	1.17205	0.19427
0.9	0.14376	1.10162	0.15973

The coefficient of power of a VAWT is directly related to the coefficient of torque by the relation

$$C_p = TSR \cdot C_q \quad (10)$$

Hereby these two parameters represent the effectiveness of the rotor in generating rotational torque, and subsequently power from the wind. However, the nature of these both are different. For both the rotors, the C_p value increases at first with TSR , reaches maximum, and then plummets. The same cannot be deduced for C_q . Coefficient of thrust quantifies the force exerted by wind on the turbine structure, which is essential for structural and foundation design for VAWTs, where the effects of asymmetric loading and torque ripples can be significant. Hence, the aerodynamic loading and drag study is essential for the structural design. From Table 5 and Table 6, it is evident that the impact of wind on savonius rotors decreases with increasing TSR , while the converge is true for bionic rotor for the given TSR range. This further suggests the usage of bio-inspired designs at the low wind conditions while pushing for optimal performance regions for savonius rotors.

Table 6: Performance of Bionic Rotor

TSR	Bionic		
	C_p	C_t	C_q
0.1	0.0095	0.39972	0.095
0.2	0.01573	0.4237	0.07865
0.3	0.01933	0.44141	0.06444
0.4	0.0089	0.456	0.02225
0.5	-0.00786	0.461	-0.01572
0.6	-0.0357	0.4769	-0.0595

The power coefficient comparison between the Savonius and bio inspired rotors reveals distinct operational characteristics with the maximum C_p for Savonius rotor being 0.285 at TSR of 0.7 while that of Bionic rotor was 0.0195 at the TSR of 0.3. In the case of the Savonius rotor, a gradual rise to peak was observed indicating an extended high performance range. For bionic rotors, there was a rapid rise to peak followed by a sharp decline at higher $TSRs$. The results illustrate that bio Inspired

rotors achieve earlier startup while the Savonius rotor shows higher peak power coefficients making Bionic rotors optimal for low speed applications.

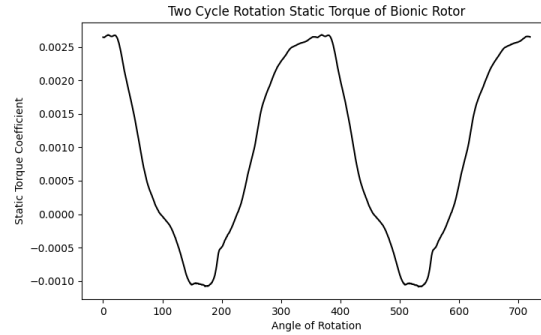


Figure 9: Static Torque of Bionic Rotor through the rotation

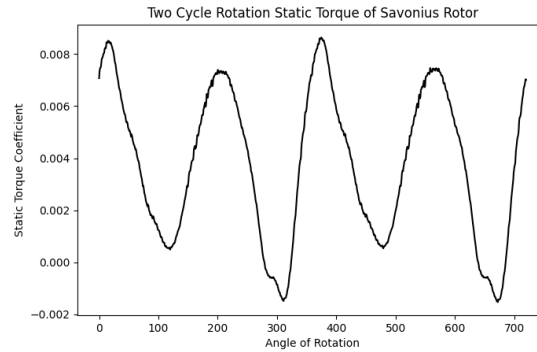


Figure 10: Static Torque of Savonius Rotor through the rotation

The static torque data gives the rotational variation of the rotor performance with the changing orientation. Figure 9 shows that Bionic rotors create the torque pattern of one peak per 360° of rotation and the flow is periodic in nature. Contrary to this, Savonius rotors boast two peaks of torque in one cycle revolution as depicted in Figure 10 showing a 180° symmetry in geometry.

These torque patterns yield many important information regarding the peak torque orientations. In savonius rotors, a peak torque when the rotor is 45° and 225° to the flow is observed from the torque plots. At angle 135° and 315°, the static torque values were minimum. Since, the bionic rotors only have one peak power per 360° cycle, the maximum torque is at 0° orientation while the minimum is at 180° with respect to the reference flow.

Vorticity contours reveal the helical nature of bio-inspired rotors that create complex three-dimensional flow patterns. The single-blade configuration generates asymmetric wake patterns, explaining the 360° torque periodicity observed in Figure 11-15.

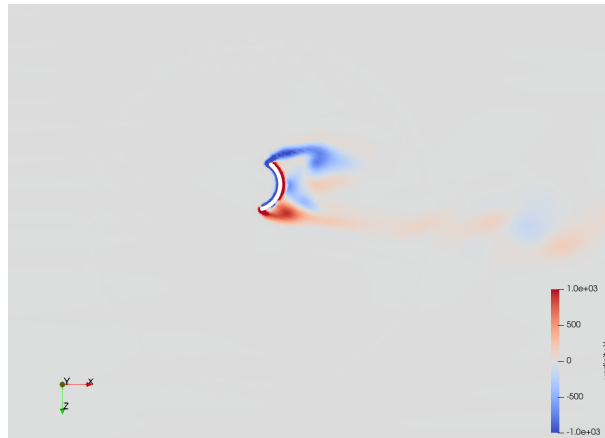


Figure 11: Vorticity Contours (a)16.6%

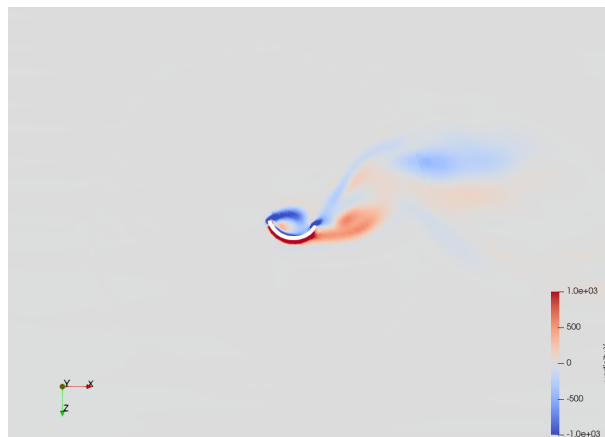


Figure 12: Vorticity Contours (b)33.3%

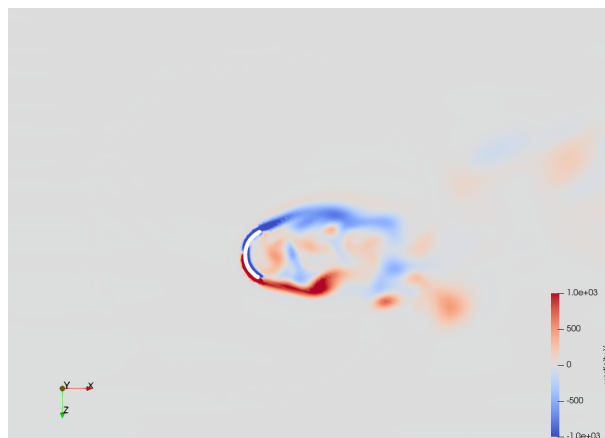


Figure 13: Vorticity Contours (c)50%

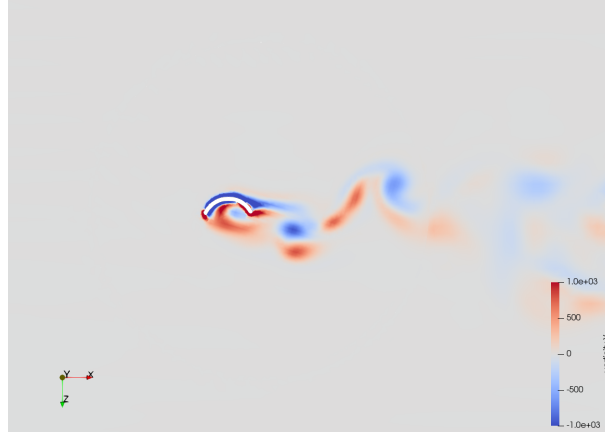


Figure 14: Vorticity Contours (d)66.6%



Figure 15: Vorticity Contours (e)83.3%

The vorticity intensity decreases from root to tip of the rotor geometry and the wake is narrow. There exists to some extent vortex shedding, the frequency of which plays a major role in torque ripple.

Reynolds number (Re) is the parameter which defines the nature of the flow. So, the variance of torque with respect to this has been studied for the TSR 0.3 of Bionic rotor and 0.7 for the savonius rotor by changing the Reynolds number from 10,000 to 100,000.

Table 7: Reynolds Number Sensitivity

Reynolds Number	Bionic C_{p_max}	% Change	Savonius C_{p_max}	% Change
10,000	0.01818	-	0.16519	-
25,000	0.01832	0.7%	0.17044	3.08%
48,000	0.01937	5.4%	0.17599	3.15%
75,000	0.01892	-2.3%	0.17591	-0.04%
100,000	0.019	0.42%	0.17827	1.32%

Table 7 pronounces increased impact of Reynolds number for savonius rotors while bionic rotors show relative insensitivity. At the normal conditions i.e. 5 m/s wind velocity and $1\text{e-}5$ air viscosity, the performance of both the rotors peak as tabulated.

4 Conclusions

This 3D numerical investigation of bio-inspired vertical axis wind turbine rotors has revealed several insights for computational approaches for this kind of problem as well as the urban wind energy applications.

1. For dynamic analysis of vertical axis wind turbine rotors, where the fluid interface changes with the turbine orientation, MRF method is not suitable to capture the flow hence requiring AMI interpolation method.
2. 3D investigation of asymmetric vertical axis wind rotors is necessary to study the torque variation with the orientation making the performance prediction more accurate.
3. The torque generation mechanism of bionic rotors vary from savonius (single peak torque pattern as compared to double peak patterns) affecting vibration characteristics and design requirements.
4. A higher solidity of savonius rotors directly correlates to a wider wake making it difficult for array configuration. However, for Bionic rotors, the wake is fairly narrower with faster recovery making it suitable for turbine fields.
5. Effects of Reynolds number are more pronounced for Savonius rotors as compared to the Bio Inspired designs.
6. The comparatively stable torque pattern of bionic rotor, compared to Savonius rotor suggests minimal stress fluctuations providing opportunities for lightweight bio-mimetic materials that align with natural stress distributions.
7. Bio Inspired rotors demonstrate superior startup characteristics with initiating wind speed 47% lower than conventional Savonius rotors. (1.5 m/s vs 2.2 m/s for studied geometry). This increased availability event at low wind speeds offsets the peak power disadvantage as compared to savonius rotors in urban application.
8. Bio-Inspired rotors provide significant room for improvement with change in helical angle and pitch optimization to improve the power coefficient while maintaining the startup advantages.

5 Acknowledgement

I would like to extend my deepest gratitude to my supervisors, Prof. Dr. Manabendra De, and Prof. Dr. Chandan Bose, for their relentless support and valuable critiques throughout this study. Their

attention to detail and academic prowess made my experience of learning and working very insightful and exemplary. My FOSSEE mentor, Mr. Manjil Sitoula, provided the necessary guidance that helped me navigate the hurdles in the progression toward the completion of this project.

I also thank the faculty of Department of Mechanical and Aerospace Engineering at Pulchowk Campus, Tribhuvan University, whose resources and assistance have been invaluable. The guidance of Dr. Sudip Bhattacharya has been essential in order to formulate CFD foundations and prepare the simulation setup for the study. Finally, a sincere acknowledgment to my peers for their camaraderie and the captivating discussions that inspired me throughout this academic experience. Their collective wisdom and encouragement have been a cornerstone of my research experience.

References

- [1] K. Golecha, M. Kamoji, S. Kedare, and S. Prabhu, “Review on savonius rotor for harnessing wind energy,” *Wind Engineering*, vol. 36, no. 6, pp. 605–645, 2012.
- [2] M. Kamoji, S. Kedare, and S. Prabhu, “Experimental investigations on the effect of overlap ratio and blade edge conditions on the performance of conventional savonius rotor,” *Wind Engineering*, vol. 32, no. 2, pp. 163–178, 2008.
- [3] M. H. Ali *et al.*, “Experimental comparison study for savonius wind turbine of two & three blades at low wind speed,” *International Journal of Modern Engineering Research (IJMER)*, vol. 3, no. 5, pp. 2978–2986, 2013.
- [4] B. D. Altan, G. Altan, and V. Kovan, “Investigation of 3d printed savonius rotor performance,” *Renewable Energy*, vol. 99, pp. 584–591, 2016.
- [5] J. B. Kalluvila and B. Sreejith, “Numerical and experimental study on a modified savonius rotor with guide blades,” *International journal of green energy*, vol. 15, no. 12, pp. 744–757, 2018.
- [6] M. Kamoji, S. B. Kedare, and S. Prabhu, “Experimental investigations on single stage modified savonius rotor,” *Applied Energy*, vol. 86, no. 7-8, pp. 1064–1073, 2009.
- [7] A. Damak, Z. Driss, and M. S. Abid, “Experimental investigation of helical savonius rotor with a twist of 180,” *Renewable Energy*, vol. 52, pp. 136–142, 2013.
- [8] N. Alom and U. K. Saha, “Influence of blade profiles on savonius rotor performance: Numerical simulation and experimental validation,” *Energy Conversion and Management*, vol. 186, pp. 267–277, 2019.
- [9] W. El-Askary, A. S. Saad, A. M. AbdelSalam, and I. Sakr, “Experimental and theoretical studies for improving the performance of a modified shape savonius wind turbine,” *Journal of Energy Resources Technology*, vol. 142, no. 12, p. 121303, 2020.
- [10] A. S. Saad, I. I. El-Sharkawy, S. Ookawara, and M. Ahmed, “Performance enhancement of twisted-bladed savonius vertical axis wind turbines,” *Energy Conversion and Management*, vol. 209, p. 112673, 2020.

- [11] P. Venkataraman and M. De Manabendra, “Numerical investigation of stand-still characteristics of a bio-inspired vertical axis wind turbine rotor,” in *IOP Conference Series: Materials Science and Engineering*, vol. 377, no. 1. IOP Publishing, 2018, p. 012014.
- [12] C. Seidel, S. Jayaram, L. Kunkel, and A. Mackowski, “Structural analysis of biologically inspired small wind turbine blades,” *International Journal of Mechanical and Materials Engineering*, vol. 12, pp. 1–9, 2017.
- [13] S. Ashwindran, A. Abd Aziz, and A. Oumer, “Unsteady computational study of novel biologically inspired offshore vertical axis wind turbine at different tip speed ratios: A two-dimensional study,” *International Journal of Automotive and Mechanical Engineering*, vol. 16, no. 2, pp. 6753–6772, 2019.
- [14] J. B. Damota, J. d. D. R. García, A. C. Casanova, J. T. Miranda, C. G. Caccia, and M. I. L. Galdo, “Analysis of a nature-inspired shape for a vertical axis wind turbine,” *Applied Sciences*, vol. 12, no. 14, p. 7018, 2022.
- [15] U. ESI-OpenCFD, “Improvement of arbitrary mesh interface (ami) algorithm for external aerodynamic simulation with rotating wheels,” *Fourth international conference in numerical and experimental aerodynamics of road vehicles and trains*, 2021.